DR YU WU (Orcid ID : 0000-0002-8250-7571)
DR ANNE SPANG (Orcid ID : 0000-0002-2387-6203)

Received Date : 03-Jul-2019
Revised Date : 10-Sep-2019
Accepted Date : 02-Jan-2020

Color : Fig 1-9

Regulation of endo-lysosomal pathway and autophagic flux by broad-spectrum anti-pathogen inhibitor ABMA

Yu Wu[1], Claire Boulogne[2], Stefan Carle[3], Maria Podinovskaia[4], Holger Barth[3], Anne Spang[4], Jean-Christophe Cintrat[5], Daniel Gillet[1]*, and Julien Barbier[1]*

[1] Service d'Ingénierie Moléculaire des Protéines (SIMOPRO), CEA, Université Paris-Saclay, LabEx LERMIT, Gif-sur-Yvette 91191, France

[2] IMAGERIE-GIF, Institute for Integrative Biology of the Cell (I_2BC), CEA, CNRS, Université Paris-Sud, Université Paris-Saclay, Gif-sur-Yvette 91191, France

[3] Institute of Pharmacology and Toxicology, University of Ulm Medical Center, Ulm 89081, Germany

[4] Growth and Development, Biozentrum, University of Basel, Basel CH-4056, Switzerland

[5] Service de Chimie Bio-organique et Marquage (SCBM), CEA, Université Paris-Saclay, LabEx LERMIT, Gif-sur-Yvette 91191, France

* Correspondence to Daniel Gillet, daniel.gillet@cea.fr and Julien Barbier, julien.barbier@cea.fr. Tel.: +33-169087646; Fax, + 33-169089071

Keywords: Broad-spectrum inhibitor; Endo-lysosomal pathway; Toxins; Autophagy

Running title: Cellular Regulation by the Broad-spectrum Inhibitor ABMA

Abbreviations

TPC_2, two-pore channel 2; HTS, high-throughput screening; TGN, trans-Golgi network; DT, diphtheria toxin; LT, lethal toxin from *Bacillus anthracis*; TcdB, toxin B from *Clostridium difficile*; TcsL, lethal toxin from *Clostridium sordellii*; HSV-2, Herpes simplex virus type 2; *Sn, Simkania negevensis; Ctr, Chlamydia trachomatis*; R, protection factor; EGF, epidermal growth factor; Tet, tetrandrine; eGFP-CRM197, His-eGFP-CRM197; DQ-BSA, DQ™ Red BSA; LC3, microtubule-associated protein 1 light chain 3; Baf A1, bafilomycin A1; TEM, transmission electron microscopy; ILVs, intraluminal vesicles.

Abstract:

The endo-lysosome system is involved in endocytosis, protein sorting and degradation as well as autophagy. Numerous toxins and pathogens exploit this system to enter host cells and exert their deleterious effects. Modulation of host endo-lysosome pathway may restrict multiple toxins intoxication as well as pathogen infection. ABMA, selected from a high-throughput screening against the cytotoxicity of ricin toxin, exhibits a broad-spectrum anti-toxin and anti-pathogen activity. Here, we show that ABMA selectively retains endocytosed protein and toxin to late endosomes, and thus delaying their intracellular trafficking. It also impairs the autophagic flux by excessive fusion of late endosomes and autophagosomes. Its exclusive action on late endosomes and corresponding consequences on the endo-lysosomal pathway and autophagic flux are distinct from known inhibitors such as bafilomycin A1, EGA or chloroquine. Hence, besides being a broad-spectrum inhibitor of endocytosed toxins and pathogens, ABMA may serve as a molecular tool to dissect endo-lysosome system-related cellular physiology and mechanisms of pathogenesis.

1. Introduction

Outbreaks of emerging pathogens without licensed treatments and with microbial drug-resistance are major public health threats [1-3]. An emerging strategy in anti-infectious drug discovery is to look for therapies targeting host functions, which are exploited by pathogens for infection and/or growth in host cells [4-13]. The endo-lysosomal system is made of dynamic organelles (early endosomes, recycling endosomes, late endosomes and lysosomes) into which cargo molecules are internalized, transported, recycled or digested for cellular homeostasis. It is a predominant pathway used by toxins and pathogens to enter host cells before escaping to the cytoplasm or, for some parasites and bacteria, building a vacuole in which they proliferate [14]. Moreover, autophagy converges into the late endosome/lysosome system through the fusion of autophagosome with endosomes and lysosomes to accomplish autophagic degradation of unnecessary or dysfunctional cellular components, which is an indispensable cellular mechanism in response to nutrition starvation, cell stress as well as pathogen infection [15].

Several chemical molecules have been identified and used as regulators of the endo-lysosome system. Dynasore as well as pitstop-1 and -2 blocks dynamin- and clathrin-dependent endocytosis [16]; EGA inhibits trafficking of toxins and pathogens in early endosomes with an unknown cellular target [11]; bafilomycin raises endosomal pH by specifically inhibiting vacuolar-type H^+-ATPase [17]; chloroquine [18] and several other inhibitors (e.g. amodiaquine [8]) block lysosomal degradation by inactivating lysosomal hydrolases; Tetrandrine inhibits lysosomal functions by specifically blocking the endo-lysosomal channel two-pore channel 2 (TPC_2) [19]. These molecules, without exception, exhibit broad-spectrum anti-pathogen activities [8, 11, 18, 20]. Furthermore, these specific molecular tools contribute substantially to the understanding of intracellular trafficking and infection mechanisms of known as well as emerging pathogens [11, 18, 21].

Previously, we performed a cell-based high-throughput screening (HTS) for inhibitors of ricin toxin and found three inhibitors [22]. Retro-1 and -2, selectively block retrograde trafficking of toxins and pathogens at the early endosome-TGN (trans-Golgi Network) interface [22]. Safety and efficacy against ricin of another hit, ABMA, has been validated in vivo [12]. Moreover, ABMA was found to protect cells against four bacterial toxins (diphtheria toxin *from Corynebacterium diphtheriae* (DT), lethal toxin from *Bacillus anthracis* (LT), toxin B from *Clostridium difficile* (TcdB), lethal toxin from *Clostridium sordellii* (TcsL)), as well as four viruses (Ebola, Rabies, Dengue-4 and Herpes simplex virus type 2 (HSV-2)), two species of Chlamydiales intracellular bacteria (*Simkania negevensis (Sn), Chlamydia trachomatis (Ctr*)) and the parasite *Leishmania infantum* at μM level [12, 23].

Here, we further demonstrate that ABMA delays endo-lysosomal trafficking at the level of late endosomes, thereby retaining endocytosed pathogens and proteins in this compartment. Furthermore, ABMA stimulates the fusion of late endosomes with autophagosomes, forming amphisomes in excess, and thus disrupting the autophagic flux. Its mechanism of action is different from known endo-lysosomal trafficking inhibitors, which suggests that ABMA is a selective tool for the study of cellular trafficking and pathogenesis.

2. Results

2.1. ABMA and EGA, two broad-spectrum inhibitors, have apparent synergistic effect to inhibit the cytotoxicity of diphtheria toxin (DT)

As described before, ABMA, a broad-spectrum inhibitor of multiple toxins and intracellular pathogens [12, 23], was selected from a cell-based HTS for inhibitors of ricin toxin [22]. ABMA induces late endosomes accumulation [12], however, how ABMA inhibits intracellular trafficking of pathogens is not yet resolved.

Another recently identified wide-spectrum anti-pathogen inhibitor, EGA, inhibits endo-lysosomal trafficking by direct action on early endosome [11]. Both compounds act on the endo-lysosomal system, but they have different anti-toxin and antiviral spectra (Table 1). For example, cytotoxic activity of toxin B from *Clostridium difficile* is acidic endosome-dependent and relies on endosomes to translocate into the cytoplasm [24, 25]. However, ABMA, not EGA, can inhibit its cytotoxicity. This suggests that ABMA and EGA act at different locations along the endo-lysosomal pathway.

In order to further analyze the mechanism of action of ABMA, we questioned whether ABMA and EGA could have additional or synergistic inhibitory effects on toxins that are sensitive to both compounds. DT is a well-identified single-pathway toxin, which relies on the acidification of endosomes at the early-late endosome interface to translocate its enzymatic domain into the cytoplasm [28, 29]. We compared the effect of each compound and their combination on the cytotoxicity of DT, at concentrations lower than their respective IC_{50}s. Protection factor (R, R= $IC_{50\ drug}$/ $IC_{50\ DMSO}$, ratio of toxin concentrations to inhibit half of maximal protein biosynthesis of cells in the presence of drug or DMSO) is used to quantify efficacy of the compound at indicated concentrations (see our previous description [12]). ABMA at 30 μM (IC_{50}: 62.5 μM [12]) and EGA at 1.25 μM (IC_{50}: 9.7 μM, Fig 1A) both inhibited DT with a protection factor (R) of ~5. The combination of the two compounds at these concentrations led to protection factors of 59.7 ± 8.5 against DT (n=3, Fig 1B and 1C) without additive toxicity (date not shown). Moreover, EGA at 2.5 μM (R: 32.9 ± 8.3) combined with ABMA at 30 μM (R: 3.9 ± 0.06) substantially improved protection factor (R: 1645 ± 262.8, n=3, Fig 1C). These values are way above the multiple of the individual protection factors, suggesting an apparent synergistic effect of the combination. This indicates that ABMA and EGA may inhibit DT cytotoxicity with different mechanism of action. Similarly, we observed that ABMA combined with dynasore (inhibitor of endocytosis) or tetrandrine (Tet, see description below) inhibited DT with largely improved R values (Fig 1D and 1E).

The epidermal growth factor (EGF), once bound to its cell-surface receptor (EGFR), is known to be internalized and to traffic along the endo-lysosomal pathway down to the lysosomes where it is degraded [30]. Thus, fluorescently labeled EGF is used as a kinetic marker of endocytosis and trafficking through the endo-lysosomal pathway until it is degraded in the lysosomes. To further dissect the kinetics of drugs' action, we investigated the trafficking of fluorescently labeled Alexa555-EGF in the presence of ABMA or EGA. A549 cells were incubated with Alexa555-EGF for 30 min to allow EGF to enter the cells by receptor-mediated endocytosis. Then, cells were incubated with the compounds for 4 h to examine the cellular trafficking of EGF (Fig 2A). ABMA substantially inhibited degradation of EGF as shown by the persistence of a strong fluorescent signal in intracellular compartments, compared to the DMSO control. In contrast, EGA barely prevented the degradation of EGF as shown by the weak fluorescent signal of intracellular compartments, similar to that of the

DMSO control. Tet, an inhibitor of lysosomal calcium channels [20], was used as a positive control of the blocking of lysosomal degradation and gave the strongest fluorescent signal of intracellular compartments after 4 h (Fig 2A). These results suggest that ABMA blocks or delays the access of internalized proteins to lysosomal degradation, while EGA acts at an early stage of EGF entry. To be note, combination of ABMA with Tet produced markedly increased efficacy in inhibiting DT cytotoxicity (Fig 1E), indicating they may act on endolysosomal pathway distinctively.

2.2. ABMA induces retention of EGF and DT in acidic endosomes, delays degradation of DQ-BSA

Knowing that ABMA restricted degradation of EGF, we then used lysotracker to label acidic organelles of live cells and found that EGF substantially co-localized with lysotracker-labeled vesicles in ABMA-treated cells (Fig 2B). This indicates that ABMA inhibits EGF degradation and leads to its accumulation in acidic organelles. As shown before, in contrast to the DMSO control, lysotracker staining was more condensed and brighter in presence of ABMA indicating an enlarged volume of endosomes (Fig 2B), which were previously characterized as Rab7-positive late endosomes [12].

Subsequently, His-eGFP-CRM197 (eGFP-CRM197, Fig 3A) was employed to monitor how ABMA interfere with the intracellular trafficking of the DT. CRM197 is a nontoxic DT that has a glycine to glutamic acid mutation at amino acid 52 in catalytic domain, resulting in the loss of enzymatic activity but without change to its intracellular trafficking [31]. The N-terminal tagging with eGFP of the toxin allows tracking of the catalytic domain along its intracellular route, which eventually translocates across endosomal membrane. As early as 45 min after incubation with A549 cells, vesicle-shaped fluorescence from eGFP-CRM197 was visualized inside cells (Fig 3B), indicating that toxins were internalized and routing to the endo-lysosomal pathway. After 5 h incubation, in the DMSO-treated control cells, the eGFP-CRM197 signal was very weak with only a few labeled intracellular vesicles. In addition, no obvious co-localization with lysotracker was observed, suggesting that most of the toxin was either degraded or had translocated from endosomal compartments to the cytosol. In contrast, in ABMA-treated cells, the eGFP-CRM197 signal was much stronger, clearly visible as punctuated vesicles in the cells and substantially co-localized with lysotracker positive-organelles (Fig 4A). Moreover, in HeLa cells stably expressing mApple-Rab7,

eGFP-CRM197 co-localized partially with mApple-Rab7 in the presence of ABMA, which was not the case in DMSO-treated control cells (Fig 4B). These data strongly suggest that ABMA inhibits trafficking of EGF and DT by trapping them in acidic and Rab7 positive-compartments, most likely late endosomes.

To further characterize the action of ABMA on endo-lysosomal degradation, we investigated degradation of red fluorescent DQ™ Red BSA (DQ-BSA) in live cells at different time points. DQ-BSA is a fluorogenic substrate for proteases, with a strong fluorescence quenching effect because it is heavily labeled with BODIPY dyes. Upon protease-mediated lysosomal hydrolysis of DQ-BSA, the dequenched fluorophores produce a bright fluorescence. Cells were pulsed with DQ-BSA for 30 min without compounds to allow cellular uptake of the labelled protein and then chased in the presence of compounds. After 2 h, fluorescence was visible in DMSO-treated cells, indicating that endocytosed DQ-BSA was hydrolyzed in lysosomes (Fig 5A and B). The signal was increased at 6 h but decreased at 18 h due to clearance of DQ-BSA fragments and fluorophore. In contrast to the DMSO control cells, ABMA-treated cells were barely fluorescent at 2 h. The signal slightly increased at 6 h, but was very intense at 18 h. Finally, cells treated with chloroquine, which also acts on late endosomes/lysosomes, persistently showed faint fluorescence at all time points (Fig 5A). These data suggest that chloroquine completely blocked degradation of DQ-BSA, whereas ABMA delayed degradation of DQ-BSA.

Lysosomal degradation is accomplished by multiple proteases. We examined the activity of cathepsin B, one of the major lysosomal proteases, in the lysate of ABMA-treated cells as well as by mixing cell lysates with ABMA. Cathepsin B fluorescent substrate was used to monitor the protease's activity. Neither ABMA treated-cells nor cell lysates freshly mixed with ABMA inhibited cleavage of cathepsin B substrate (Fig 5C), suggesting that ABMA does not influence lysosomal proteases directly or indirectly, in a cell-dependent way. In contrast, chloroquine-treated cells exhibited an apparent decreased fluorescence, indicating that chloroquine diminishes cathepsin B activity in a cell-dependent way. Consistently, the immunofluorescence intensities of cathepsin D were not influenced by ABMA (Fig 5D).

Altogether, these data demonstrate that the mechanism of action of ABMA is distinct from that of the known lysosome inhibitor chloroquine (Fig 5). ABMA delays endo-lysosomal trafficking of endocytosed cargoes by trapping them in acidic and Rab7-positive compartments rather than inhibiting their lysosomal degradation.

2.3. ABMA upregulates LC3II and p62, enhances colocalization of p62 with late endosome markers Rab7 and Rab9

Macroautophagy, herein referred to as autophagy, is an alternative degradative process in which cytosolic proteins or intracellular organelles are sequestered within double-membrane structures called autophagosomes for digestion. Precisely, autophagosomes either first fuse with late endosomes to form amphisomes, which subsequently fuse with lysosomes, or they fuse directly with lysosomes to generate autolysosomes [32], but the latter is primarily based on the yeast system [33]. It is clear now that in mammalian cells, several stages of endocytic pathway contribute to efficient autophagy [33]. Since ABMA acts on late endosomes, we questioned whether ABMA can thus regulate autophagy.

The LC3 protein (microtubule-associated protein 1 light chain 3) is used to monitor autophagy. Lipidation of LC3 I to LC3 II is an obligatory process for autophagosome expansion and formation. We first evaluated whether ABMA changes cellular LC3 I and LC3 II levels by immunoblot. Apparently, ABMA (30μM) strongly increased endogenous LC3 II in A549 cells (Fig 6A), HeLa cells (data not shown) as well as murine RAW 264.7 cells (Fig 6C). The action of ABMA on LC3 II increment initiated as early as 0.5 h and continued up to 4 - 6 h (Fig 6C). Notably, the upregulation of LC3 II could be induced by the activation of autophagy, or alternatively, by inhibition of autophagic degradation [34].Thus, SQSTM1/p62 (hereinafter p62), an autophagy substrate, was monitored in parallel with LC3. Activation of autophagy will accelerate p62 degradation, we also observed that SMER-28, a small molecule of autophagy activator[35], induced p62 degradation; while bafilomycin A1 (Baf A1), autophagic flux blocker, oppositely increased p62 protein level (Fig 6B). Importantly, ABMA increased the level of p62 in a time-dependent manner, suggesting a possible inhibition of the autophagic degradation (Fig 6C). To further explore the effect of ABMA on autophagic flux, we added Baf A1 (100 or 200 nM) in the last 4 hours of ABMA incubation (Fig 6D). ABMA and Baf A1 alone both largely increased LC3 II compared to DMSO control (10.47± 1.55-fold for ABMA at 60

μM; 5.43 ± 0.60 and 5.88 ± 0.39-fold for 100 nM and 200 nM of Baf A1). Importantly, addition of Baf A1 in the cells treated with ABMA only induced a limited increase of LC3 II (with Baf A1 (100 nM): 13.49 ± 1.82-fold; with Baf A1 (200 nM): 11.28 ± 0.94-fold). This further indicates that ABMA inhibits autophagic flux in a downstream step like Baf A1.

Next, we used HeLa cells stably expressing GFP-LC3B [36] to investigate the effect of ABMA on the autophagic process. LC3B is one of isoforms of LC3, which is equally distributed throughout the cytoplasm and also localized in the nucleolar region [37]. ABMA increased GFP-LC3B puncta in a dose-dependent way (data not shown). In addition, we compared the effect of chloroquine as well as a combination of chloroquine and ABMA on GFP-LC3B level. Chloroquine has long been used to inhibit autophagic flux in the late stage. The combined addition of ABMA and chloroquine did not further increase the number or size of GFP-LC3B puncta (Fig 6E, n.s $p>0.05$), suggesting that similarly to chloroquine, ABMA acts in the late stage to regulate autophagy by inhibiting the autophagic degradation.

p62, as an autophagic substrate, incorporates into completed autophagosomes and is then degraded in autolysosomes [38]. ABMA induced an upregulation of p62 by immunoblotting (Fig 6A and 6C). Finding out in which specific compartment the undegraded p62 is accumulated can help us to better understand the action of ABMA on autophagy. Accordingly, we examined co-localization of increased p62 with endosome/lysosome marker proteins Rab7, Rab9 and Lamp1. As we found before, Rab7 protein fluorescence was largely increased by ABMA, rather than EEA1 and Lamp1 [12]. Importantly, the two upregulated proteins, Rab7 and p62, were strongly co-localized (Fig 7A and 7D), increased co-localization of LC3 and Rab7 were also observed (see description below). Immunostaining of another late endosomal protein, Rab9, also significantly enhanced its immunofluorescence in the presence of ABMA and colocalized with p62 (Fig 7B and 7D). In contrast, the lysosome marker Lamp1 was not influenced by ABMA and did not enhance its co-localization with p62 (Fig 7C and 7D). Considering enhanced co-localization of p62 with the late endosome markers Rab7 and Rab9, we hypothesized that ABMA increases the level of the p62 protein by inhibiting its autophagic degradation. This defective autophagic degradation could be due to its accumulation in amphisomes, which result from the fusion of autophagosomes with late

endosomes. Then, it is only when amphisomes subsequently fuse with lysosomes to generate autolysosomes that materials wrapped inside can be degraded properly by lysosomal hydrolases.

2.4. ABMA stimulates the fusion of late endosomes with autophagosomes and disrupts the autophagic flux

To further support our hypothesis that ABMA interferes with autophagic degradation by influencing amphisomes rather than autolysosomes, ultrastructure morphology of ABMA-treated HeLa cells stably expressing GFP-LC3B (Fig 8A) was investigated by transmission electron microscopy (TEM). In addition, immunogold labeled antibodies against GFP were employed to investigate localization of GFP-LC3B. As shown in Fig 8B, cells stably expressing GFP-LC3B exhibited numerous double-membrane autophagic compartments in the presence of ABMA, which were absent in DMSO-treated cells. These autophagic compartments were further identified by the presence of GFP-LC3B recognized by immunogolds (Fig 8B, right panel). Notably, immunogolds specific for GFP-LC3B were present in autophagic compartment as well as nascent autophagophore (Fig 8B, right panel, white arrow). Moreover, as we found before in A549 cells [12], ABMA induced accumulation of MVBs/late endosomes (Fig 8B, arrowhead), which are characterized by round or near-round shape with variable intraluminal vesicles (ILVs). Particularly, MVBs/late endosomes were localized mostly in the proximity of autophagic compartments suggesting that because of ABMA, late endosomes are recruited for autophagy and destined to fuse with autophagic compartments. This further suggests that ABMA leads to the accumulation of late endosomes, enhances consequently the formation of amphisomes by their fusion with autophagosomes but disrupts the autophagic flux.

3. Discussion

Small-molecule inhibitors of intracellular trafficking have emerged in cell biology studies to explore cellular physiology as well as pathogenesis of various disease-inducing agents, especially pathogen-host interactions [16, 18, 20, 21, 39, 40]. Compared to dominant-negative or genetic modulation of specific proteins involved in trafficking, chemical reagents harbor particular advantages to regulate trafficking, e.g. their high specificity, acute action and insusceptibility resistance to compensatory mechanisms [11, 16].

The specific target of ABMA is currently unknown, but the data presented here suggest that its broad-spectrum anti-toxin and anti-pathogen activity is related to the restriction of endo-lysosomal trafficking at the site of late endosomes (Fig 9). Its mechanism of action is distinct from that of several other known inhibitors. Because of their distinct mechanisms, the combination of these known inhibitors (EGA (Fig 1B), dynasore and tetrandrine (Fig 1D and 1E) as well as Baf A1 [12]) with ABMA produced markedly increased efficacy in inhibiting DT cytotoxicity. Our results suggest that ABMA may be used as a selective tool for the studies of late endosome-related pathways and function. We anticipate that specific modulation of late endosomes by ABMA, combined with other inhibitors acting on alternative sites of intracellular trafficking may help to better elucidate entry mechanisms of pathogens.

Late endosomes are considered as essential sorting stations for protein and lipid transport, as well as for entry and development of pathogens [14, 41, 42]. Besides their role in the endocytic pathway, late endosomes have been shown to have important roles in autophagic processes [15]. Especially, Rab7 activation plays a unique role in the maturation of autophagosomes [43] and the fusion of autophagosomes and amphisomes with lysosomes [15].

In this study, we made further observations as the consequences of cell treatment by ABMA: 1) p62 avoids autophagic degradation but substantially co-localizes with late endosome protein markers Rab7 and Rab9, rather than Lamp1 (lysosome marker); 2) cells accumulate autophagic compartments shown by TEM, which are characterized by double-membrane, abundance of intraluminal GFP-LC3B and undegraded intracellular components but lack of electron-dense degraded materials and single membrane (characteristic of autolysosome); 3) autophagic compartments apparently surrounded by MVBs/late endosomes accumulate in cells. As a result, we suggest that ABMA stimulates amphisomes formation, where p62 (Fig 7) and LC3 (Fig 8) are accumulated and stalled for autophagic degradation (Fig 9).

Deficiency in the autophagic flux can be induced by multiple inhibitors [44], e.g. 3-MA (PI_3K inhibitor, inhibiting autophagosome formation), bafilomycin and chloroquine (endosome acidification inhibitor, impairing fusion of autophagosomes with lysosomes and autolysosome degradation) [45], leupeptin and E-64d (lysosomal protease inhibitors, inhibiting autophagic degradation) [46]. To our

knowledge, ABMA is the first identified molecule to disrupt the autophagic flux by regulating late endosomes and subsequent amphisomes although its precise mechanism is not resolved. This specific tool may help to better understand the function and the structure of the amphisome as well as of the entire autophagy process.

Being a broad-spectrum anti-pathogen inhibitor, ABMA exhibits variable efficacy according to the tested pathogen. Generally, it inhibits viruses (Ebola, Dengue-4 and HSV-2) and parasite (intra-macrophagic *Leishmania infantum amastigotes*) more powerfully (IC_{50s} < 10 μM) than toxins (IC_{50s} > 60 μM for DT, TcdB and lethal toxin)[12, 23]. This implies that ABMA's action on late endosomes may generate multifaceted consequences, which are more productive and selective to restrict infection and/or development of certain viruses and parasites. Mounting studies have demonstrated that autophagy can be hijacked by viruses and parasites for their infection of cells and survival [47, 48], and thus, regulation of autophagy may serve as an alternative strategy for anti-infectious treatment [49]. Further research is needed to clarify the relevance of autophagy regulation by ABMA to its inhibitory mechanism on viral and parasitic infection.

In conclusion, ABMA is not only a host-targeted inhibitor for toxins, bacteria, viruses and parasites but also a potent tool for dissecting infection mechanism of known or emerging pathogens at the level of endocytic and autophagic processes.

4. Materials and Methods

4.1. Materials and reagents

1-adamantyl (5-bromo-2-methoxybenzyl) amine (ABMA) was purchased from Chembridge (ID: 5570320, San Diego, CA, USA). The following products were purchased from the indicated commercial sources: L-[^{14}C(U)]-leucine was from Perkin-Elmer; DMSO (D4540), DT (D0564), bafilomycin A1 (B1793), Hoechst 33342 (14533), filipin III (F4767), Gelatin (G7765), EGA (SML1006), G418 (G8168), SMER28 (S8197), anti-LC3B (L7543, 1:2000 WB), anti-p62 (P0067, 1:1000 WB), anti-Lamp1 (L1418, 1:100 IF) were purchased from Sigma; anti-Rab9 (#5118, 1:200 IF) was from cell signaling; Anti-Rab7 (ab137029, 1:200 IF), anti-actin (ab3280, 1:2000 WB) and Cathepsin B Activity Assay Kit (ab65300) were from Abcam; LysoTracker Deep Red (L12492,

1:10000 IF), DQ™ Red BSA (D-112051, 10µg/ml IF), Alexa555-EGF (E-35350, 10 µg/mL IF), Anti-Cathepsin D (PA5-17353, 1:200 IF) were from ThermoFisher Scientific; anti-p62 (H00008878-M01, 1:200 IF) was from Abnova; anti-GFP antibody (ab6556, 1:20 TEM) was from Abcam and Goat-anti-rabbit IgG (H+L) antibody coupled with 10 nm gold particles (810.011, 1:20 TEM) was from Aurion. A549 and HeLa cells (ATCC) were cultured in DMEM with 10% fetal bovine serum (FCS). HeLa cells stably expressing GFP-LC3B were grown in RPMI with 10% FCS and 500 µg/mL G418 [50]. HeLa cells stably expressing mApple-Rab7 were grown in high-glucose DMEM with 10% FCS and 1% sodium pyruvate. All cells were authenticated, checked for contamination and cultured at 37°C with 5% CO_2.

4.2 Toxin intoxication assays

For detailed experimental procedures, see previous description [12]. Briefly, A549 cells in the presence of various concentrations of compounds solubilized in DMSO (final DMSO concentration was 0.1% in controls and in treated cells) were incubated with increasing doses of DT in 96-well Cytostar-TTM scintillating bottom plates (Perkin Elmer). After 20 h, the medium was replaced with DMEM without leucine (Eurobio) containing 10% fetal bovine serum, 2 mM L-glutamine, 0.1 mM non-essential amino acids, supplemented with 0.5 µCi/mL [^{14}C]-leucine. The cells were grown for an additional 4 h at 37 °C and then protein biosynthesis was determined by measuring the incorporation of radiolabeled-leucine into cells using a Wallac 1450 MicroBeta scintillation counter (Perkin-Elmer).

Drug concentration was plotted against the corresponding percentage of protection of cells, and the 50% efficacy concentration (EC_{50}) was calculated by nonlinear regression using the Prism software package (Graphpad Inc., San Diego, CA).

4.3 Molecular cloning, expression and affinity purification of recombinant His-eGFP-CRM197 (eGFP-CRM197)

Basis for molecular cloning was the plasmid pTRC99A-myc-DTE148S, which was kindly gifted by Dr. Emmanuel Lemichez (Paris, France). pTRC99A-His-DTG52E also known as pTRC99A-His-CRM197 was created using site directed mutagenesis and overhang PCR with traditional cloning techniques. eGFP was amplified from a plasmid kindly gifted by Dr. Joachim Orth/Dr. Klaus Aktories

(Freiburg, Germany) and inserted into pTRC99A-His-CRM197 using In-Fusion® (Clontech) cloning resulting in pTRC99A-His-eGFP-CRM197, which includes a GSG-linker between eGFP and CRM197.

The expression plasmid pTRC99A-His-eGFP-CRM197 was transformed into competent Shuffle® T7 Express (NEB). A single clone was picked for over day culture in 5 mL LB-Amp (LB medium [tryptone 10 g/L, yeast extract 5 g/L, NaCl 10 g/L] containing Ampicillin [100 mg/L]) at 30 °C and 180 rpm. The culture was then transferred into an Erlenmeyer flask with 120 mL fresh LB-Amp for overnight culture at 30 °C and 180 rpm. The following day, two Erlenmeyer flasks with 1 L of LB-Amp each were inoculated with 50 mL of overnight culture per flask and further incubated at 30 °C and 180 rpm. Upon reaching OD600 of 0.4 the expression was induced using 1 mM IPTG and temperature was shifted to 16 °C for overnight incubation at 180 rpm. Cultures were centrifuged at 5500 g for 7 min. Pellets were resuspended in equilibration buffer (Tris-HCl 50 mM, NaCl 300 mM, imidazole 20 mM, pH 7.5) and frozen. Subsequently, pellets were thawed, supplied with 1 mM PMSF, stored on ice and sonicated (10 pulses with 30 s and amplitude of ~ 40 % with intermediate pauses of 30 s on ice). The solution was then centrifuged at 13000 g for 30 min at 4 °C and filtered through 0.45 µm and 0.2 µm syringe filters. Purification was performed using an ÄKTA® FPLC system with a 1 mL Ni-NTA column. Protein was then eluted with elution buffer (Tris-HCl 50 mM, NaCl 300 mM, imidazole 500 mM, pH 7.5), protein containing fractions were pooled and buffer was exchanged to PBS using Vivaspin 20® centrifugal concentrators with 30 kDa MWCO (3 times refilled with PBS). Protein was further stored at -80 °C.

4.4 Generation of HeLa cells stably expressing mApple-Rab7

HeLa CCL2 cells (ATCC) were maintained in DMEM supplemented with 10% fetal calf serum (BioConcept, Switzerland), 2 mM L-glutamine, 1 mM sodium pyruvate, and penicillin and streptomycin antibiotics). mApple-Rab7a was a gift from Michael Davidson (Addgene plasmid #54945; http://n2t.net/addgene:54945; RRID: Addgene_54945). The mApple-Rab7 plasmid was linearized using the AseI restriction enzyme (NEB), and transfected into HeLa cells using TurboFect transfection reagent (Thermo Fisher). Medium was supplemented with 500 µg/mL G418 (G8168, Sigma) selection antibiotic 48 h later. Twenty days post transfection, mApple-positive cells were

sorted by FACS ARIA III (Biozentrum FACS Core Facility) and re-sorted 15 days later into 96-well plates for single cell clonal expansion. A healthy clone displaying characteristic Rab7 distribution was selected for further experiments.

4.5 Immunocytochemistry

Cells were grown on glass coverslips one day before experiments. Following treatments, cells were rinsed with PBS, fixed with 4% paraformaldehyde-PBS for 20 min at room temperature or with methanol at -20°C for 10 min. After three washes with PBS, cells were permeabilized with 0.1% saponin for 5 min. Subsequently, cells were blocked in 0.5% gelatin-PBS and then stained with antibodies. Finally, the coverslips were mounted on glass slides and imaged using an inverted microscope (Ti-U, Nikon) or confocal microscope (SP8X, Leica) with a 63X PLAN APO oil-immersion objective. The co-localization analysis was quantified according to Pearson's correlation coefficient of two interested proteins by Image J software with JACop plug-in [51].

4.6 EGF and eGFP-CRM197 trafficking

Cells were incubated with Alexa555-EGF (10 μg/mL) for 30 min and then washed three times with PBS before being treated with compounds for the indicated time. eGFP-CRM197 (1:150) (37°C, 5% CO_2) was added with compounds into cells for indicated time. Images of live cells were obtained as same as *4.3*.

4.7 DQ-BSA degradation

A549 cells were incubated with DQ-BSA (DQ™ Red BSA) at a concentration of 10 μg/mL for 30 min (37°C, 5% CO_2). The cells were then washed three times with PBS before being treated with compounds for the indicated time. Photographs of live cells were obtained using an inverted microscope (Ti-U, Nikon).

4.8 TEM

HeLa cells stably expressing GFP-LC3B were incubated with ABMA or DMSO for 24 h. Next, cells were fixed for 90 min at room temperature with 2% paraformaldehyde and 0.1% glutaraldehyde in 0.1

M phosphate buffer (pH 7.4), then they were washed with 0.1 M phosphate buffer (pH 7.4) and detached from the flask by gently scrapping. Cells were centrifuged (1200 g, 2 min) in 2% low melting point agarose to obtain concentrated pellets in 1 mm^3. Dehydration was performed at 4°C with 10%, 30% and 50% ethanol baths, and then at -20°C with 70%, 90% and 100% ethanol baths. Samples were finally kept in absolute ethanol before the embedding process. Embedding in graded series (25-50-75-100-100-100%) of resin (LR White Resin, Agar Scientific, Oxford instruments) mixed with ethanol was processed on 3 days at -20°C. Subsequently, blocs were polymerized for 24 h at -20°C and for 24 h at RT under UV light. Ultrathin sections (80 nm) were cut by an ultramicrotome EM UC6 (Leica Microsystems) and collected on Formvar carbon-coated nickel grids.

Immunogold labelling was performed as follows. Ultrathin sections were pretreated with PBS-Tween20 0.5% for 5 min, PBS-Glycine 50 mM for 5 min twice, and then blocked in a blocking solution for goat-gold conjugates (Aurion) for 30 min followed by washing with PBS-BSA-c™ (Aurion, 900.099). The anti-GFP primary antibody diluted in PBS-BSA-c (1:20) was employed on sections for 1 h. Sections were washed with PBS four times, with PBS-BSA-c twice, then incubated with the Goat-anti-rabbit IgG (H+L) secondary antibody coupled with 10 nm gold particles for 30 min. Finally, sections were washed with PBS four times and ten times with water before staining in uranyl acetate (8 min) and lead citrate (2 min).

Observations were made with a JEOL JEM-1400 transmission electron microscope operating at 80 kV. Images were acquired using a postcolumn high-resolution (11 megapixels) high-speed camera (SC1000 Orius; Gatan) and processed with Digital Micrograph (Gatan) and Image J.

References

1. Bekerman, E. & Einav, S. (2015) Infectious disease. Combating emerging viral threats, *Science.* **348**, 282-3.

2. Jones, K. E., Patel, N. G., Levy, M. A., Storeygard, A., Balk, D., Gittleman, J. L. & Daszak, P. (2008) Global trends in emerging infectious diseases, *Nature.* **451**, 990-994.

3. Clark, G. C., Casewell, N. R., Elliott, C. T., Harvey, A. L., Jamieson, A. G., Strong, P. N. & Turner, A. D. (2019) Friends or Foes? Emerging Impacts of Biological Toxins, *Trends Biochem Sci.* **44**, 365-379.

4. Kaufmann, S. H. E., Dorhoi, A., Hotchkiss, R. S. & Bartenschlager, R. (2017) Host-directed therapies for bacterial and viral infections, *Nature reviews Drug discovery*, 35-56.

5. Gupta, N., Noel, R., Goudet, A., Hinsinger, K., Michau, A., Pons, V., Abdelkafi, H., Secher, T., Shima, A., Shtanko, O., Sakurai, Y., Cojean, S., Pomel, S., Lievin-Le Moal, V., Leignel, V., Herweg, J. A., Fischer, A., Johannes, L., Harrison, K., Beard, P. M., Clayette, P., Le Grand, R., Rayner, J. O., Rudel, T., Vacus, J., Loiseau, P. M., Davey, R. A., Oswald, E., Cintrat, J. C., Barbier, J. & Gillet, D. (2017) Inhibitors of retrograde trafficking active against ricin and Shiga toxins also protect cells from several viruses, Leishmania and Chlamydiales, *Chem Biol Interact.* **267**, 96-103.

6. Czyz, D. M., Potluri, L. P., Jain-Gupta, N., Riley, S. P., Martinez, J. J., Steck, T. L., Crosson, S., Shuman, H. A. & Gabay, J. E. (2014) Host-directed antimicrobial drugs with broad-spectrum efficacy against intracellular bacterial pathogens, *MBio.* **5**, e01534-14.

7. Zilbermintz, L., Leonardi, W., Tran, S. H., Zozaya, J., Mathew-Joseph, A., Liem, S., Levitin, A. & Martchenko, M. (2016) Cross-inhibition of pathogenic agents and the host proteins they exploit, *Sci Rep.* **6**, 34846.

8. Zilbermintz, L., Leonardi, W., Jeong, S. Y., Sjodt, M., McComb, R., Ho, C. L., Retterer, C., Gharaibeh, D., Zamani, R., Soloveva, V., Bavari, S., Levitin, A., West, J., Bradley, K. A., Clubb, R. T., Cohen, S. N., Gupta, V. & Martchenko, M. (2015) Identification of agents effective against multiple toxins and viruses by host-oriented cell targeting, *Sci Rep.* **5**, 13476.

9. Tam, J., Beilhartz, G. L., Auger, A., Gupta, P., Therien, A. G. & Melnyk, R. A. (2015) Small molecule inhibitors of Clostridium difficile toxin B-induced cellular damage, *Chemistry & biology.* **22**, 175-85.

10. Saenz, J. B., Doggett, T. A. & Haslam, D. B. (2007) Identification and characterization of small molecules that inhibit intracellular toxin transport, *Infection and Immunity.* **75**, 4552-4561.

11. Gillespie, E. J., Ho, C. L., Balaji, K., Clemens, D. L., Deng, G., Wang, Y. E., Elsaesser, H. J., Tamilselvam, B., Gargi, A., Dixon, S. D., France, B., Chamberlain, B. T., Blanke, S. R., Cheng, G., de la Torre, J. C., Brooks, D. G., Jung, M. E., Colicelli, J., Damoiseaux, R. & Bradley, K. A. (2013) Selective inhibitor of endosomal trafficking pathways exploited by multiple toxins and viruses, *Proc Natl Acad Sci U S A.* **110**, E4904-12.

12. Wu, Y., Pons, V., Goudet, A., Panigai, L., Fischer, A., Herweg, J. A., Kali, S., Davey, R. A., Laporte, J., Bouclier, C., Yousfi, R., Aubenque, C., Merer, G., Gobbo, E., Lopez, R., Gillet, C., Cojean, S., Popoff, M. R., Clayette, P., Le Grand, R., Boulogne, C., Tordo, N., Lemichez, E., Loiseau, P. M., Rudel, T., Sauvaire, D., Cintrat, J. C., Gillet, D. & Barbier, J. (2017) ABMA, a small molecule that inhibits intracellular toxins and pathogens by interfering with late endosomal compartments, *Sci Rep.* **7**, 15567.

13. Schor, S. & Einav, S. (2018) Combating Intracellular Pathogens with Repurposed Host-Targeted Drugs, *ACS Infect Dis.* **4**, 88-92.

14. Gruenberg, J. & van der Goot, F. G. (2006) Mechanisms of pathogen entry through the endosomal compartments, *Nat Rev Mol Cell Biol.* **7**, 495-504.

15. Fader, C. M. & Colombo, M. I. (2009) Autophagy and multivesicular bodies: two closely related partners, *Cell Death Differ.* **16**, 70-8.

16. von Kleist, L., Stahlschmidt, W., Bulut, H., Gromova, K., Puchkov, D., Robertson, M. J., MacGregor, K. A., Tomilin, N., Pechstein, A., Chau, N., Chircop, M., Sakoff, J., von Kries, J. P., Saenger, W., Krausslich, H. G., Shupliakov, O., Robinson, P. J., McCluskey, A. & Haucke, V. (2011) Role of the Clathrin Terminal Domain in Regulating Coated Pit Dynamics Revealed by Small Molecule Inhibition (vol 146, pg 471, 2011), *Cell.* **146**, 841-841.

17. Bowman, E. J., Siebers, A. & Altendorf, K. (1988) Bafilomycins - a Class of Inhibitors of Membrane Atpases from Microorganisms, Animal-Cells, and Plant-Cells, *P Natl Acad Sci USA.* **85**, 7972-7976.

18. Akpovwa, H. (2016) Chloroquine could be used for the treatment of filoviral infections and other viral infections that emerge or emerged from viruses requiring an acidic pH for infectivity, *Cell Biochem Funct.* **34**, 191-196.

19. Sakurai, Y., Kolokoltsov, A. A., Chen, C. C., Tidwell, M. W., Bauta, W. E., Klugbauer, N., Grimm, C., Wahl-Schott, C., Biel, M. & Davey, R. A. (2015) Ebola virus. Two-pore channels control Ebola virus host cell entry and are drug targets for disease treatment, *Science.* **347**, 995-8.

20. Bhagya, N. & Chandrashekar, K. R. (2016) Tetrandrine - A molecule of wide bioactivity, *Phytochemistry.* **125**, 5-13.

21. Schnell, L., Mittler, A. K., Sadi, M., Popoff, M. R., Schwan, C., Aktories, K., Mattarei, A., Tehran, D. A., Montecucco, C. & Barth, H. (2016) EGA Protects Mammalian Cells from Clostridium difficile CDT, Clostridium perfringens Iota Toxin and Clostridium botulinum C2 Toxin, *Toxins.* **8**, 101.

22. Stechmann, B., Bai, S. K., Gobbo, E., Lopez, R., Merer, G., Pinchard, S., Panigai, L., Tenza, D., Raposo, G., Beaumelle, B., Sauvaire, D., Gillet, D., Johannes, L. & Barbier, J. (2010) Inhibition of retrograde transport protects mice from lethal ricin challenge, *Cell.* **141**, 231-42.

23. Dai, W., Wu, Y., Bi, J., Wang, S., Li, F., Kong, W., Barbier, J., Cintrat, J. C., Gao, F., Gillet, D., Su, W. & Jiang, C. (2018) Antiviral Effects of ABMA against Herpes Simplex Virus Type 2 In Vitro and In Vivo, *Viruses.* **10**, 119.

24. Jank, T., Belyi, Y. & Aktories, K. (2015) Bacterial glycosyltransferase toxins, *Cell Microbiol.* **17**, 1752-65.

25. Tao, L., Zhang, J., Meraner, P., Tovaglieri, A., Wu, X., Gerhard, R., Zhang, X., Stallcup, W. B., Miao, J., He, X., Hurdle, J. G., Breault, D. T., Brass, A. L. & Dong, M. (2016) Frizzled proteins are colonic epithelial receptors for C. difficile toxin B, *Nature.* **538**, 350-355.

26. Tehran, D. A., Zanetti, G., Leka, O., Lista, F., Fillo, S., Binz, T., Shone, C. C., Rossetto, O., Montecucco, C., Paradisi, C., Mattarei, A. & Pirazzini, M. (2015) A Novel Inhibitor Prevents the Peripheral Neuroparalysis of Botulinum Neurotoxins, *Sci Rep.* **5**, 17513.

27. Schnell, L., Mittler, A. K., Mattarei, A., Tehran, D. A., Montecucco, C. & Barth, H. (2016) Semicarbazone EGA Inhibits Uptake of Diphtheria Toxin into Human Cells and Protects Cells from Intoxication, *Toxins.* **8**, 221.

28. Lemichez, E., Bomsel, M., Devilliers, G., vanderSpek, J., Murphy, J. R., Lukianov, E. V., Olsnes, S. & Boquet, P. (1997) Membrane translocation of diphtheria toxin fragment - A exploits early to late endosome trafficking machinery, *Molecular Microbiology.* **23**, 445-457.

29. Leka, O., Vallese, F., Pirazzini, M., Berto, P., Montecucco, C. & Zanotti, G. (2014) Diphtheria toxin conformational switching at acidic pH, *Febs Journal.* **281**, 2115-2122.

30. Dunn, W. A., Connolly, T. P. & Hubbard, A. L. (1986) Receptor-mediated endocytosis of epidermal growth factor by rat hepatocytes: receptor pathway, *J Cell Biol.* **102**, 24-36.

31. Giannini, G., Rappuoli, R. & Ratti, G. (1984) The amino-acid sequence of two non-toxic mutants of diphtheria toxin: CRM45 and CRM197, *Nucleic Acids Res.* **12**, 4063-9.

32. Nakamura, S. & Yoshimori, T. (2017) New insights into autophagosome-lysosome fusion, *Journal of Cell Science.* **130**, 1209-1216.

33. Tooze, S. A., Abada, A. & Elazar, Z. (2014) Endocytosis and autophagy: exploitation or cooperation?, *Cold Spring Harb Perspect Biol.* **6**, a018358.

34. Klionsky, D. J.Abdelmohsen, K.Abe, A.Abedin, M. J.Abeliovich, H.Arozena, A. A.Adachi, H.Adams, C. M.Adams, P. D.Adeli, K.Adhihetty, P. J.Adler, S. G.Agam, G.Agarwal, R.Aghi, M. K.Agnello, M.Agostinis, P.Aguilar, P. V.Aguirre-Ghiso, J.Airoldi, E. M.Ait-Si-Ali, S.Akematsu, T.Akporiaye, E. T.Al-Rubeai, M.Albaiceta, G. M.Albanese, C.Albani, D.Albert, M. L.Aldudo, J.Algul, H.Alirezaei, M.Alloza, I.Almasan, A.Almonte-Beceril, M.Alnemri, E. S.Alonso, C.Altan-Bonnet, N.Altieri, D. C.Alvarez, S.Alvarez-Erviti, L.Alves, S.Amadoro, G.Amano, A.Amantini, C.Ambrosio, S.Amelio, I.Amer, A. O.Amessou, M.Amon, A.An, Z. Y.Anania, F. A.Andersen, S. U.Andley, U. P.Andreadi, C. K.Andrieu-Abadie, N.Anel, A.Ann, D. K.Anoopkumar-Dukie, S.Antonioli, M.Aoki, H.Apostolova, N.Aquila, S.Aquilano, K.Araki, K.Arama, E.Aranda, A.Araya, J.Arcaro, A.Arias, E.Arimoto, H.Ariosa, A. R.Armstrong, J. L.Arnould, T.Arsov, I.Asanuma, K.Askanas, V.Asselin, E.Atarashi, R.Atherton, S. S.Atkin, J. D.Attardi, L. D.Auberger, P.Auburger, G.Aurelian, L.Autelli, R.Avagliano, L.Avantaggiati, M. L.Avrahami, L.Awale, S.Azad, N.Bachetti, T.Backer, J. M.Bae, D. H.Bae, J. S.Bae, O. N.Bae, S. H.Baehrecke, E. H.Baek, S. H.Baghdiguian, S.Bagniewska-Zadworna, A., et al. (2016) Guidelines for the use and interpretation of assays for monitoring autophagy (3rd edition), *Autophagy.* **12**, 1-222.

35. Sarkar, S., Perlstein, E. O., Imarisio, S., Pineau, S., Cordenier, A., Maglathlin, R. L., Webster, J. A., Lewis, T. A., O'Kane, C. J., Schreiber, S. L. & Rubinsztein, D. C. (2007) Small molecules enhance autophagy and reduce toxicity in Huntington's disease models, *Nat Chem Biol.* **3**, 331-8.

36. Bampton, E. T., Goemans, C. G., Niranjan, D., Mizushima, N. & Tolkovsky, A. M. (2005) The dynamics of autophagy visualized in live cells: from autophagosome formation to fusion with endo/lysosomes, *Autophagy.* **1**, 23-36.

37. Koukourakis, M. I., Kalamida, D., Giatromanolaki, A., Zois, C. E., Sivridis, E., Poulilioul, S., Mitrakas, A., Gatter, K. C. & Harris, A. L. (2015) Autophagosome Proteins LC3A, LC3B and LC3C Have Distinct Subcellular Distribution Kinetics and Expression in Cancer Cell Lines, *Plos One.* **10**, e0137675.

38. Itakura, E. & Mizushima, N. (2011) p62 targeting to the autophagosome formation site requires self-oligomerization but not LC3 binding, *Journal of Cell Biology.* **192**, 17-27.

39. Nonnenmacher, M. E., Cintrat, J. C., Gillet, D. & Weber, T. (2015) Syntaxin 5-dependent retrograde transport to the trans-Golgi network is required for adeno-associated virus transduction, *J Virol.* **89**, 1673-87.

40. Klausner, R. D., Donaldson, J. G. & Lippincott-Schwartz, J. (1992) Brefeldin A: insights into the control of membrane traffic and organelle structure, *J Cell Biol.* **116**, 1071-80.

41. Marquer, C., Tian, H., Yi, J., Bastien, J., Dall'Armi, C., Yang-Klingler, Y., Zhou, B., Chan, R. B. & Di Paolo, G. (2016) Arf6 controls retromer traffic and intracellular cholesterol distribution via a phosphoinositide-based mechanism, *Nat Commun.* **7**, 11919-11932.

42. Jackson, C. L., Walch, L. & Verbavatz, J. M. (2016) Lipids and Their Trafficking: An Integral Part of Cellular Organization, *Dev Cell.* **39**, 139-153.

43. Zhan, L., Chen, S., Li, K., Liang, D., Zhu, X., Liu, L., Lu, Z., Sun, W. & Xu, E. (2017) Autophagosome maturation mediated by Rab7 contributes to neuroprotection of hypoxic preconditioning against global cerebral ischemia in rats, *Cell Death Dis.* **8**, e2949.

44. Wang, C., Hu, Q. & Shen, H. M. (2016) Pharmacological inhibitors of autophagy as novel cancer therapeutic agents, *Pharmacol Res.* **105**, 164-75.

45. Klionsky, D. J., Elazar, Z., Seglen, P. O. & Rubinsztein, D. C. (2008) Does bafilomycin A(1) block the fusion of autophagosomes with lysosomes?, *Autophagy.* **4**, 849-850.

46. Cheng, Y., Ren, X. C., Hait, W. N. & Yang, J. M. (2013) Therapeutic Targeting of Autophagy in Disease: Biology and Pharmacology, *Pharmacol Rev.* **65**, 1162-1197.

47. Choi, Y., Bowman, J. W. & Jung, J. U. (2018) Autophagy during viral infection - a double-edged sword, *Nature Reviews Microbiology.* **16**, 340-353.

48. Thomas, S. A., Nandan, D., Kass, J. & Reiner, N. E. (2018) Countervailing, time-dependent effects on host autophagy promotes intracellular survival of Leishmania, *Journal of Biological Chemistry.* **293**, 2617-2630.

49. Chiramel, A. I., Dougherty, J. D., Nair, V., Robertson, S. J. & Best, S. M. (2016) FAM134B, the Selective Autophagy Receptor for Endoplasmic Reticulum Turnover, Inhibits Replication of Ebola Virus Strains Makona and Mayinga, *J Infect Dis.* **214**, S319-S325.

50. Mouna, L., Hernandez, E., Bonte, D., Brost, R., Amazit, L., Delgui, L. R., Brune, W., Geballe, A. P., Beau, I. & Esclatine, A. (2016) Analysis of the role of autophagy inhibition by two complementary human cytomegalovirus BECN1/Beclin 1-binding proteins, *Autophagy.* **12**, 327-42.

51. Bolte, S. & Cordelieres, F. P. (2006) A guided tour into subcellular colocalization analysis in light microscopy, *J Microsc.* **224**, 213-32.

Table 1. **Known anti-toxin and anti-pathogen spectra of ABMA and EGA** [8, 12, 21, 23, 26, 27]

Effect on toxins and pathogens		**EGA**	**ABMA**
Toxins	Positive	Lethal toxin from *Bacillus anthracis* (LT) Diphtheria toxin (DT) Exotoxin A (PE) from *P. aeruginosa* Botulinum neurotoxin A, B, C2 and D (BoNT/A, B, C2 and D) from *Clostridium botulinum* neurotoxins Iota toxin from *Clostridium perfringens* C2 toxin from *Clostridium botulinum* Cytolethal distending toxins from *Haemophilus ducreyi* (Hd-CDT) and *Clostridium difficile* (CDT)	Ricin toxin Diphtheria toxin (DT) Lethal toxin from *Bacillus anthracis* (LT) Toxin B from *Clostridium difficile* (TcdB) Lethal toxin from *Clostridium sordellii* (TcsL)
	negative	Ricin toxin Cytolethal distending toxins from *Escherichia. coli* (Ec-CDT) Toxins A and B from *Clostridium difficile*	Shiga-like toxin 2 (Stx2) from *Escherichia. coli* Botulinum neurotoxin A (BoNT/A) from *Clostridium botulinum* neurotoxins
Viruses	positive	Influenza A virus Vesicular stomatitis virus (VSV) Lymphocytic choriomeningitis virus (LCMV)	Ebola virus Rabies virus Dengue 4 virus Herpes simplex virus-2 (HSV-2)
	negative	Amphotropic murine leukemia virus (A-MLV) Nipah virus (NiV)	Chikungunya virus
Intracellular bacteria	positive	n. d	*Simkania negevensis* *Chlamydia trachomatis*
Parasites	positive	n. d	*Leishmania*

Figure Legends

Figure 1. Combination of ABMA and EGA substantially improves inhibitory effect on cytotoxicity of DT in A549 cells. (A) EGA inhibits cytotoxicity of diphtheria toxin (DT) by measuring the incorporation of [^{14}C] labeled-leucine into newly synthesized proteins in A549 cells with an EC_{50} of 9.67 μM. Results are from one representative experiment (n=2). (B) ABMA (30 μM), EGA (1.25 μM) and combination of both reversed DT-induced protein biosynthesis inhibition. Each point corresponds to mean ± S.E.M. from a representative experiment (n=3). (C) Protection factors (R) of ABMA (30 μM), EGA (1.25 μM (B) or 2.5 μM) and of their combination on cytotoxicity of DT. Results are shown as mean ± S.E.M. from 3 independent experiments. (D) Dynasore (80 μM) and (E) tetrandrine (Tet, 7.5 μM) both have apparent synergistic effects with ABMA (30 μM) in inhibiting cytotoxicity of DT. Right: R values of each drug and their combination are from one representative experiment (n=2). Experimental procedure is as same as Fig 1B, except that dynasore was employed in serum-free medium to sustain its activity, and intoxication time was 6 h.

Figure 2. ABMA induces accumulation of EGF in acidic compartments. (A) A549 cells were pulsed with Alexa555-EGF for 30 min at 37°C and then chased for 4 h at 37°C in presence of DMSO, ABMA (60 μM), EGA (30 μM) or Tet (7.5 μM) respectively. Live-cell images were obtained with an inverted microscope (Ti-U, Nikon). Representative images are from one of three experiments. Right, Fluorescence intensity of at least 30 cells from each condition was quantified and analyzed by Image J. Results are shown as mean ± S.E.M., A.U means arbitrary unit. Statistical significance was tested using unpaired t-test with Welch's correction, compared to DMSO control (n.s, $p > 0.05$; * $p < 0.05$; *** $p < 0.001$). (B) A549 cells were pulsed for 30 min at 37°C with Alexa555-EGF and chased in the presence of DMSO or ABMA for 4 h. Hoechst 33342 (blue) and Lysotracker Green (B) were added during the last 30 min of incubation. Right, Pearson's coefficients of two fluorescence were analyzed by Image J software with JACop plug-in. Values are shown as mean ± S.E.M. from 25-30 cells of two independent experiments. Statistical significance was tested using unpaired t-tests with Welch's correction (*** $p < 0.001$). Scale bar, 10 μm.

Figure 3. Identification of His-eGFP-CRM197 (eGFP-CRM197). (A) Purified protein was identified by SDS-PAGE and Coomassie blue staining. BSA at indicated concentrations was used as quantification control. (B) Intracellular fluorescence of eGFP-CRM197. A549 cells were pulsed with eGFP-CRM197 (1:150) for 45 min and directly observed by an inverted microscope (Ti-U, Nikon). Images shown are representative of two independent experiments. Scale bar, 10 μm.

Figure 4. ABMA induces accumulation of catalytically inactive DT mutant (eGFP-CRM197) in acidic compartments. A549 cells (A) or HeLa cells stably expressing mApple-Rab7 (B) were pulsed with eGFP-CRM197 (1: 150) for 5 h in complete medium in the presence of DMSO or 60 μM ABMA. Hoechst 33342 (blue) and Lysotracker DeepRed (A) was added during the last 30 min. Images of live cells were obtained by confocal microscopy (SP8X, Leica). Right, Pearson's correlation coefficients were analyzed as same as Fig 2B. Statistical significance was tested using unpaired t-tests with Welch's correction (*** $p < 0.001$). Scale bar, 10 μm.

Figure 5. ABMA delays but does not block degradation of DQ-BSA. (A) A549 cells were pulsed with DQ-BSA for 30 min at 37°C, then chased in the presence of DMSO, ABMA (60μM) or CQ (60μM) for the indicated time (n=3). Live cells were imaged by an inverted microscope (Ti-U, Nikon). Scale bar, 10 μm. (B) Fluorescence intensity of at least 30 cells was quantified and analyzed by Image J. Results are shown as mean ± S.E.M. from one representative experiment (n=3). A.U means arbitrary unit. Statistical significance was tested using unpaired t-tests with Welch's correction, compared to DMSO control (** $p < 0.01$; *** $p < 0.001$). (C) Cathepsin B activity assay. Cell-free assay: A549 cell lysate mixed with cathepsin B substrate labeled with fluorescent probe, was incubated with DMSO, ABMA (60 μM) or cathepsin B inhibitor (positive control, provided with the kit) for 1 h (left). Cell-dependent assay: lysates from A549 cells treated 24 h with compounds (ABMA or CQ, both at 60 μM) were incubated with cathepsin B substrate for 1 h. Fluorescence intensity (Ex/Em

= 400/505 nm) from cleaved fluorescent substrate was determined by imaging reader (Cytation 5, Biotek). Cathepsin B substrate replaced by buffer was used as blank control. Data represent the mean ± S.D. from duplicate well of one representative experiment (n=2), normalized to DMSO treatment. (D) Immunofluorescence of cathepsin D from A549 cells incubated with DMSO or ABMA (60 μM) for 18 h. Images were obtained by confocal microscopy (SP8X, Leica), and images shown are representative of three experiment. Scale bar, 10 μm.

Figure 6. ABMA upregulates LC3 II and p62 level. (A) Immunoblot of LC3 and p62 from lysates of A549 cells treated with ABMA at 30 μM for 16 h. (B) Immunoblot of p62 from A549 cell lysates which are respectively treated by DMSO, Baf A1 (100 nM) or SMER 28 (45 μM) for 5 h. Loading amount is examined by total proteins of each lysates imaged and analyzed by Gel Doc™ EX system (BIO-RAD). p62 amounts normalized to total loading proteins is shown as mean ± S.E.M. from 2 independent experiments. (C) Immunoblot of LC3 and p62 from lysates of RAW264.7 treated with ABMA at 30 μM for the indicated time. LC3 II and p62 (A and C) were quantified and normalized to actin, shown as mean ± S.E.M. (n=3). Statistical significance compared to 0 h was tested using paired t-tests (n.s, $p > 0.5$; *$p < 0.05$; ** $p < 0.01$; *** $p < 0.001$). (D) Autophagic flux with Baf A1 was analyzed by LC3 protein monitoring. ABMA (60 μM, 20h) incubated-A549 cells were treated with 100 nM or 200 nM Baf A1/without (-) Baf A1 during last 4h. Quantification of relative LC3 II/Actin was shown as mean ± S.E.M. (n=2). (E) HeLa cells stably expressing GFP-LC3B were incubated with chloroquine (CQ, 60 μM), or both CQ and ABMA (60 μM) for 16 h. Green fluorescence puncta and their sizes of at least 30 cells were analyzed by Image J. Statistical significance was tested using unpaired t-tests with Welch's correction (n.s, $p > 0.5$; *$p < 0.05$; ** $p < 0.01$; *** $p < 0.001$). Scale bar, 10 μm.

Figure 7. ABMA impairs degradation of p62 and enhances its localization in Rab7 and Rab9-positive vesicles. Immunostaining for Rab7 (A), Rab9 (B) or Lamp1 (C) and p62 in A549 cells pre-treated in DMSO or ABMA (60 μM) for 18 hr. Nuclei were stained with DAPI (blue). Scale bar, 10 μm. (D) Pearson`s coefficients of two proteins were analyzed by

Image J software with JACop plug-in. Values from at least 30 cells of 3 independent experiments are shown as mean ± S.E.M, statistical significance was tested using unpaired t-tests with Welch's correction, compared to DMSO control (n.s, $p > 0.5$; *** $p < 0.001$).

Figure 8. ABMA impairs autophagic flux by accumulation of amphisomes. HeLa cells stably expressing GFP-LC3B were incubated for 24 h with ABMA (30 μM) or DMSO as control. (A) Immunofluorescence of Rab7 and GFP-LC3B. Images shown are representative of two experiment obtained by confocal microscopy (SP8X, Leica). Scale bar, 10 μm. (B) Cells were processed for electron microscopy and stained by anti-GFP antibodies followed by immuno-gold labelling. Representative electron micrographs of sections are shown. Arrowheads indicate MVBs/late endosomes and arrows indicate immuno-gold labelled GFP-LC3B.

Figure 9. Model depicting the role of ABMA in the regulation of endo-lysosomal pathway and autophagic flux as well as its role as a pharmacological inhibitor of toxin translocation in mammalian cells.

Author Contributions: Y.W., D.G., J.B. conceived and designed the experiments; Y.W. performed the cell biological experiments and cytotoxicity assay of toxin; Y.W and C.B. performed TEM; S.C. and H.B. generated and identified eGFP-CRM197; M.P. and A.S. generated and identified HeLa cells stably-expressing mApple-Rab7; J.-C.C. supplied compounds; Y.W. and J.B. analyzed the data; Y.W., J.B. and D.G. wrote the paper.

Acknowledgments: We thank Dr. Aviva Tolkovsky (Cambridge Centre for Brain repair, Cambridge, UK) as well as Prof. Audrey Esclatine (University of Paris-Saclay, France) for providing HeLa cells stably-expressing GFP-LC3B, and Cynthia Gillet (Institute for Integrative Biology of the Cell, CNRS, France) for technical helps with TEM. H.B. thanks Dr. Emmanuel Lemichez (Institut Pasteur, France) for kindly providing plasmids. This work was funded by the Joint ministerial program of R&D against CBRNE risks and CEA. SIMOPRO and SCBM are members of the Laboratory of Excellence LERMIT supported by a grant from the Agence Nationale de la Recherche (*ANR-10-LABX-33*), RetroLeishma project R3, and under Contract ANR-18-CE18-0016. TEM work was done at the electron microscopy facility of Imagerie-Gif, (http://www.i2bc.paris-saclay.fr), member of IBiSA (http://www.ibisa.net), supported by "France-BioImaging" (*ANR-10-INBS-04-01*) and the Labex "Saclay Plant Science" (*ANR-11-IDEX-0003-02*). M.P. an A.S. were founded by Swiss National Science Foundation (CRII3_141956). The work in the H.B. group was supported by the German Research Foundation (DFG) project number 316249678-CRC 1279/project C02. S.C. is a member of the International Graduate School in Molecular Medicine Ulm (IGradU) and thanks IGradU for the support.

Conflicts of Interest: The authors declare no competing or financial interests.

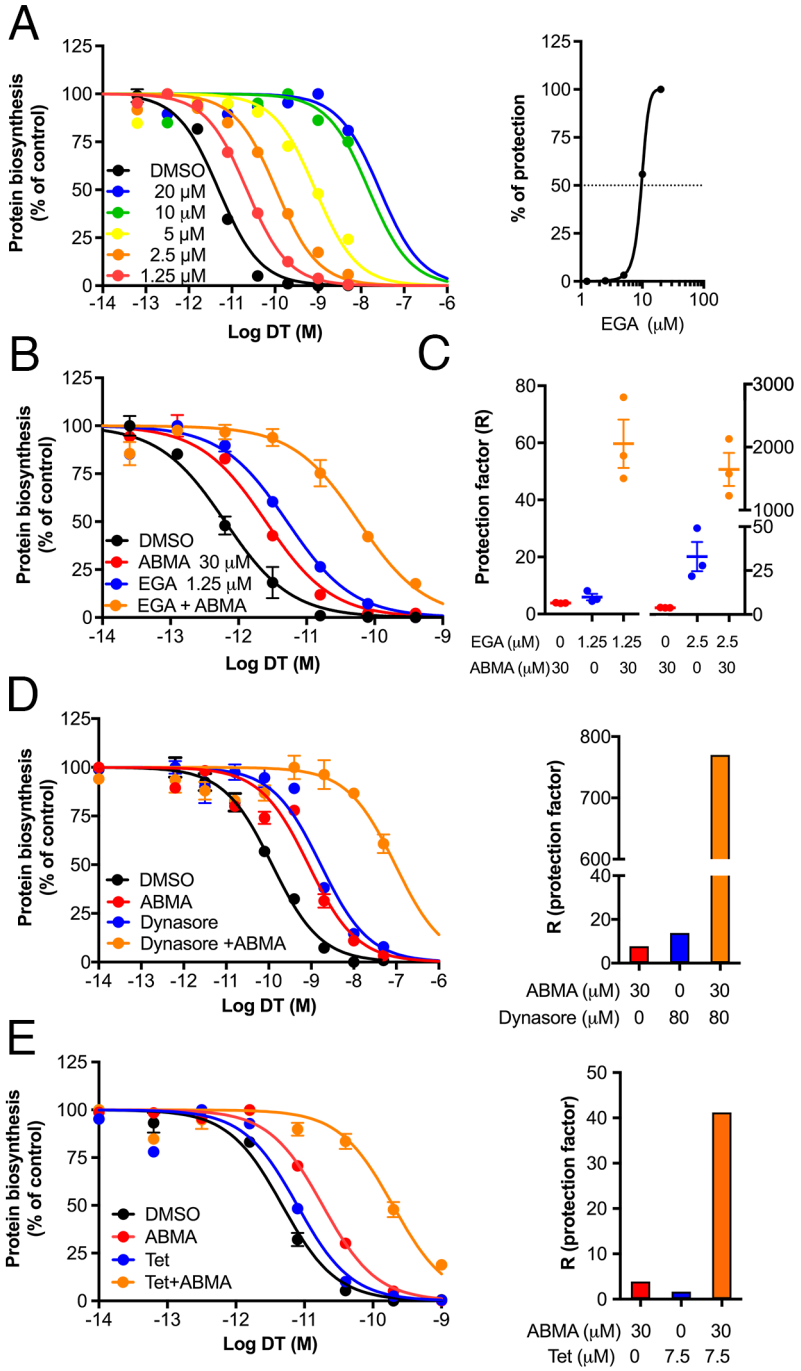

febs_15201_f1.tif

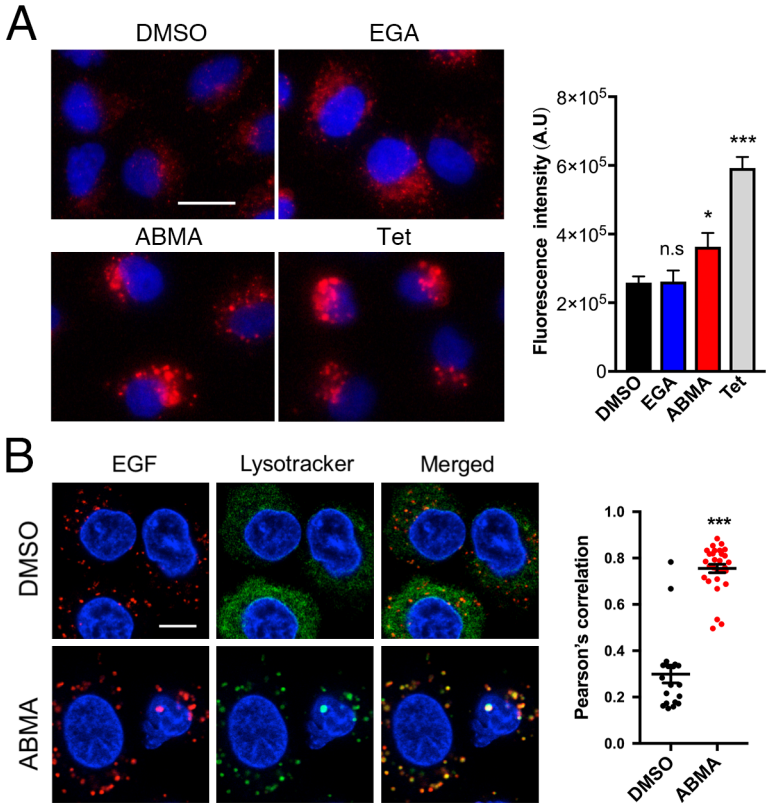

febs_15201_f2.tif

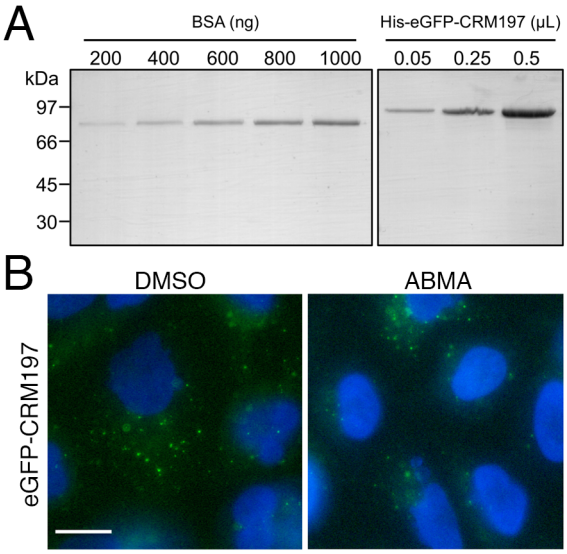

febs_15201_f3.tif

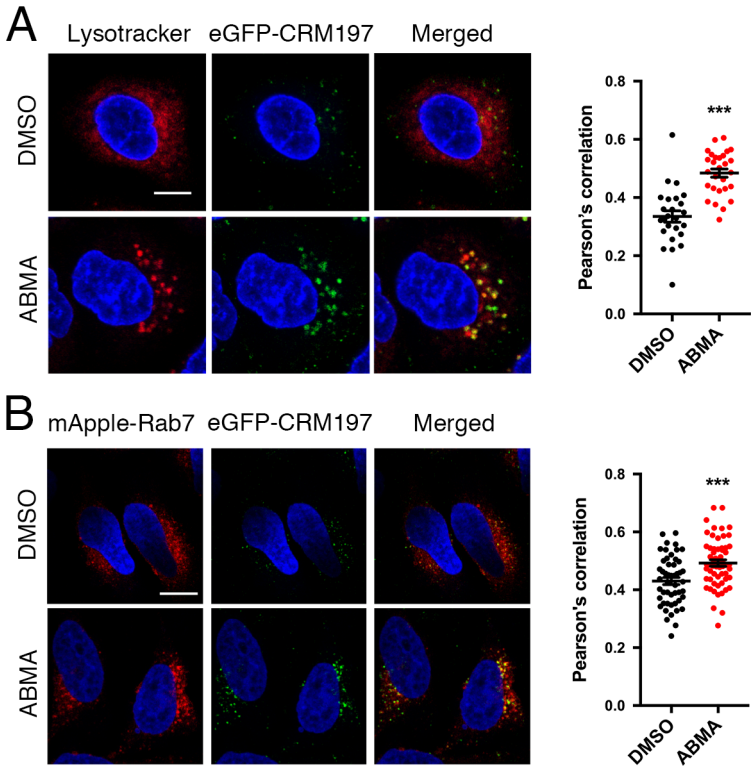

febs_15201_f4.tif

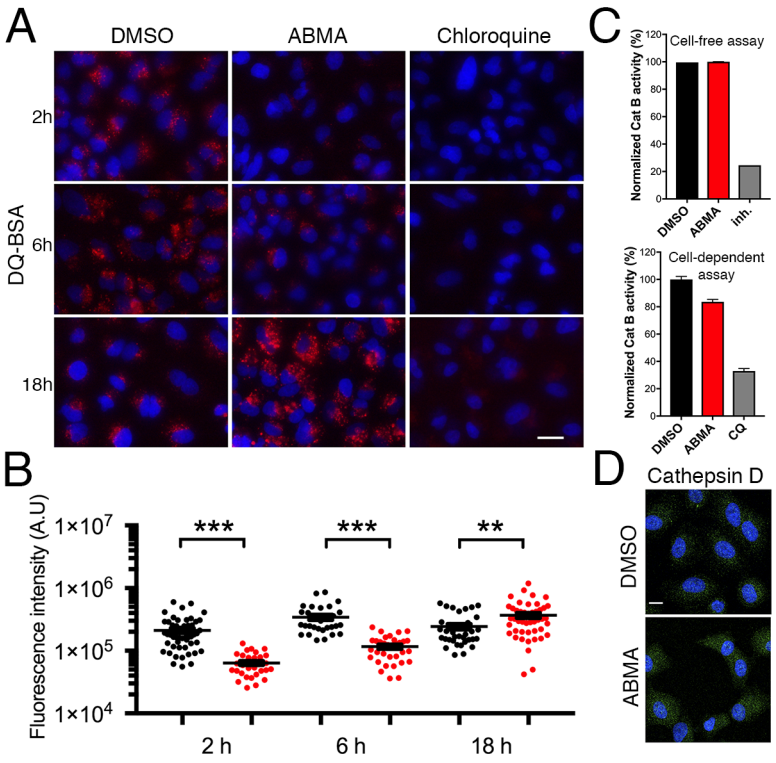

febs_15201_f5.tif

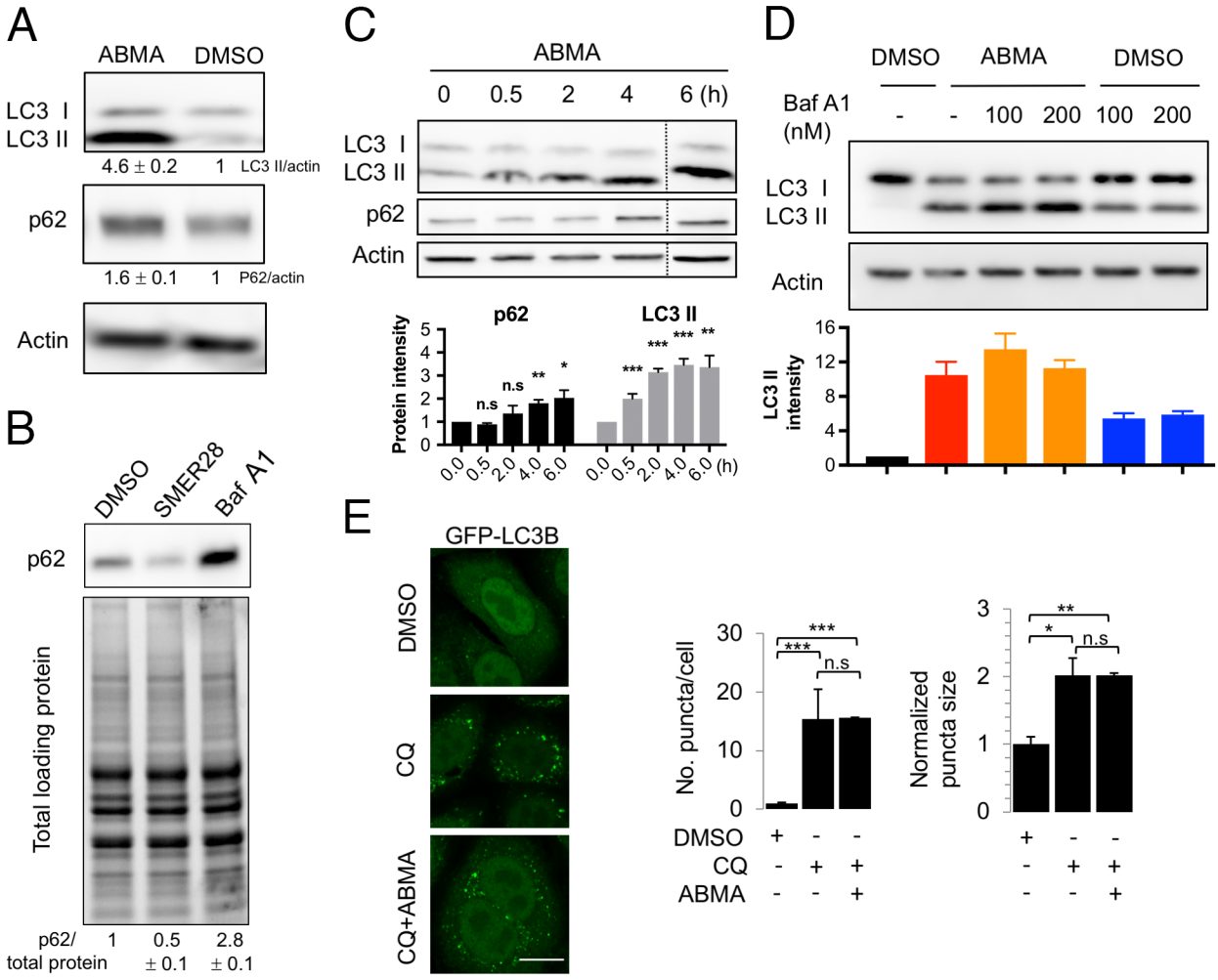

febs_15201_f6.tif

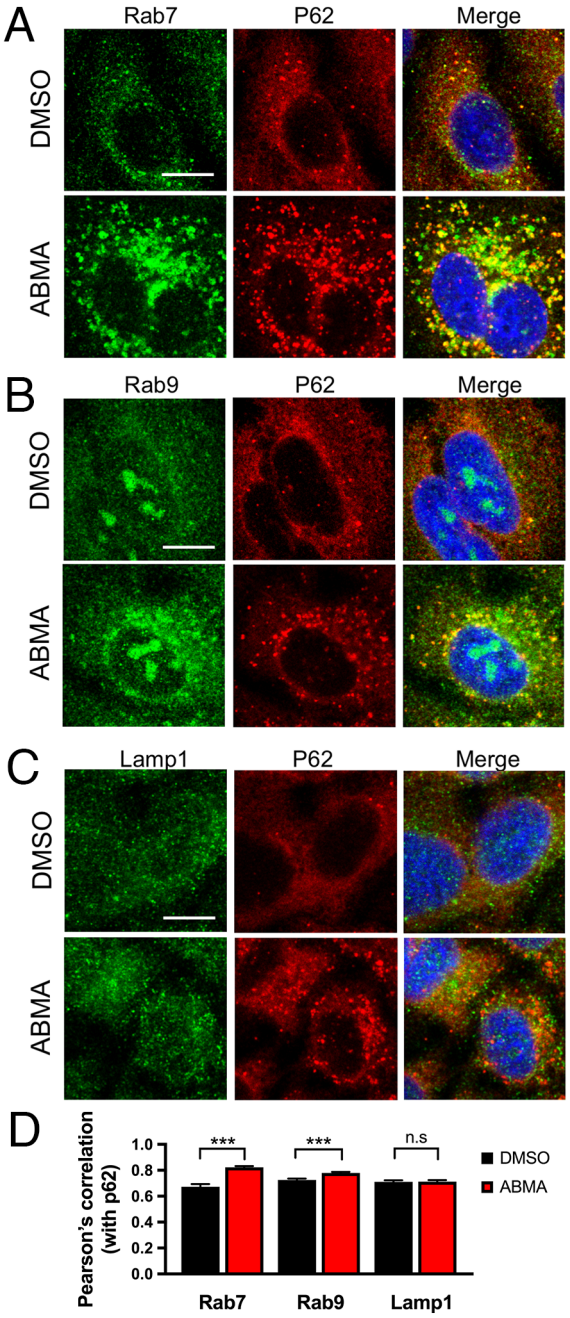

febs_15201_f7.tif

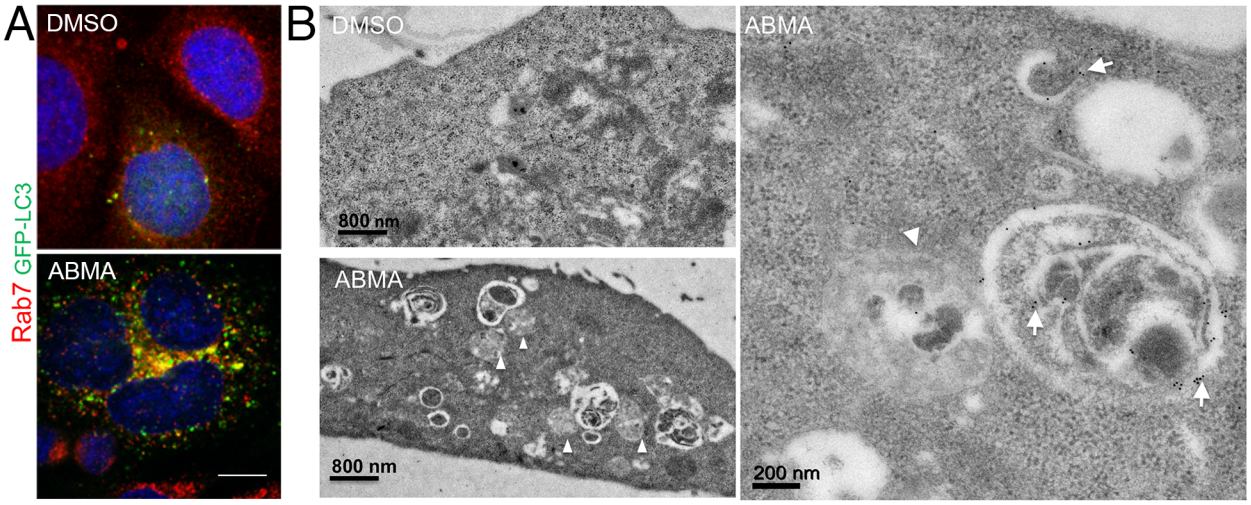

febs_15201_f8.tif

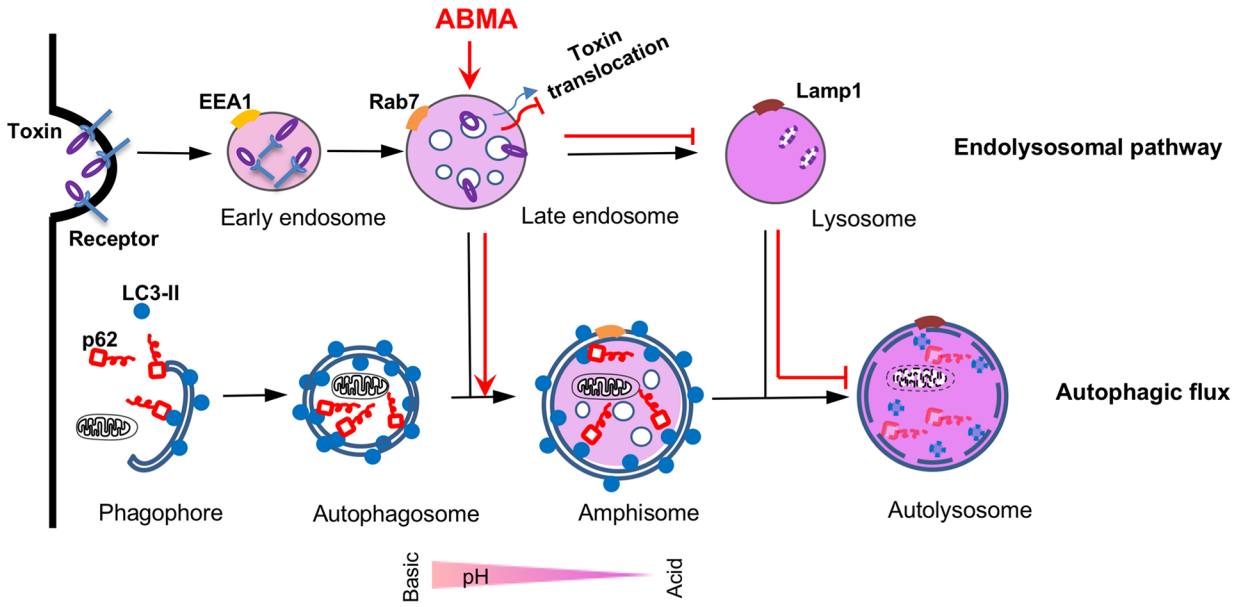

febs_15201_f9.tif